Supplementary Information for
Rational ligand choice extends the SABRE substrate scope

Johannes F. P. Colell[a‡], Angus W. J. Logan[a‡], Zijian Zhou[a], Jacob R. Lindale[a], Raul Laasner[b], Roman V. Shchepin[c], Eduard Y. Chekmenev[d,e], Volker Blum[a,b], Warren S. Warren[a,f]*, Steven J. Malcolmson[a]* and Thomas Theis[a,g,h]*

[a.] *Department of Chemistry, Duke University, Durham, NC 27708, USA.*
[b.] *Department of Mechanical Engineering and Materials Science, Duke University, Durham, NC 27708, USA.*
[c.] *Department of Chemistry, Biology, and Health Sciences, South Dakota School of Mines and Technology, Rapid City, South Dakota 57701, USA*
[d.] *Russian Academy of Sciences, Leninskiy Prospekt 14, 119991 Moscow, Russia.*
[e.] *Department of Chemistry, Integrative Biosciences (IBio), Karmanos Cancer Institute (KCI), Wayne State University, Detroit, MI 48202, USA.*
[f.] *Departments of Physics, Radiology and Biomedical Engineering, Duke University, Durham, NC 27707, USA.*
[g.] *Department of Chemistry, North Carolina State University, Raleigh, NC 27695*
[h.] *Joint Department of Biomedical Engineering University of North Carolina at Chapel Hill and North Carolina State University, Chapel Hill, NC, USA*
‡ These authors contributed equally.

Corresponding Authors
Steven J. Malcolmson, steven.malcolmson@duke.edu
Warren Warren, warren.warren@duke.edu
Thomas Theis, ttheis@ncsu.edu

Table of contents

5) Field dependence of polarisation build-up

6) Application to other nuclei

7) H-D exchange in 2-fluoropyridine

1) Synthesis of $[Ir(COD)(Phox)]PF_6$

The catalyst $[Ir(COD)(Phox)]PF_6$ (Phox = 2-(2-(diphenylphosphaneyl)phenyl)-4,5-dihydrooxazole, COD = 1,5-Cyclooctadiene) (**S1**) is readily prepared in a four-step process using published procedures.[1-4]

2) Supporting calculations

a. Technical parameters

Supporting DFT calculations were carried out using FHI-aims[5-7], a high-precision[8, 9] implementation of electronic structure theory for molecular and condensed phase systems, and use the Tkatchenko-Scheffler[10] van der Waals corrected PBE[11] functional as well as the hybrid M06 functional[12] (for comparison), both of which have been subject to extensive benchmark studies regarding their accuracy for molecular conformation and energetics in the past.[12-18] Additionally, we also quantified the approximate effects of a solvent using a recently benchmarked implicit solvation formalism[19], showing that our main conclusions remain unaffected by such a modification.

The geometries were relaxed using the *tier 2* basis sets with *tight* integration grids[5] until the modulus of any force components on the nuclei was below 10^{-2} eV/Å. Two exchange-correlation parameterizations were considered: the PBE[11] functional with the Tkatchenko-Scheffler van der Waals correction[10] ("PBE+TS") and, for compounds of particular interest, we additionally compared results to the M06-x meta-generalized gradient approximation based functional[12]. The M06-x total energies were evaluated based on fixed geometries obtained using the PBE+TS approach. The two functionals led to the same qualitative results regarding the ordering of total energies of the relaxed geometries, which were optimized for each functional and structure. Scalar relativity was handled in the atomic ZORA approximation, specifically defined in Eqs. (55) and (56) of Ref.[5]

In our additional calculations using an implicit solvent model[19], the solvent was chosen to be methanol (dielectric constant 32.7 at room temperature). The solvent model calculations are based on the relaxed geometries from the PBE+TS density functional without solvent; the total energy including the solvent model was then re-evaluated for the fixed geometry and is denoted "PBE+TS+Sol" in this supporting information. The isosurface density of the solvent model was set to 0.0125 $Å^{-3}$. Non-electrostatic parameters α and β in the model were determined as fitting parameters to the T2+T3 set of molecules as described in Ref.[19]. We use α and β of 0.0028 eV/$Å^2$ and -0.00223 eV/$Å^3$. Additional convergence parameters for the electrostatic part of the energy due to solvent were the following. The multipole

expansion orders of the polarisation potential inside and outside the cavity were set to 12 and 6, respectively. The ratio of the number of rows to columns in left-hand side matrix of the MPE equation was set to 5. In Tables (Tables S1-S3), numerical convergence of electrostatic solvation energies as a function of these parameters is demonstrated for structure (3a) of Figure 2A in the main paper, which is denoted as "conformer 1" throughout this supporting information.

Table S1. Electrostatic energy of structure (3a) (conformer 1) as a function of expansion order of the polarisation potential inside the cavity of the implicit solvent model used. See Reference[19] for implementation details.

Order	Energy [eV]
8	-1.4411
10	-1.4506
12	-1.4571
14	-1.4610

Table S2. Electrostatic energy of structure (3a) (conformer 1) as a function of expansion order of the polarisation potential outside of the cavity of the implicit solvent model used. See Reference[19] for implementation details.

Order	Energy [eV]
7	-1.4571
6	-1.4571
5	-1.4567
4	-1.4563

Table S3. Electrostatic energy of structure (3a) (conformer 1) as a function of the degree of determination, i.e., the ratio of number of rows to columns in the left-hand side matrix of the MPE equation in Eqs (15) and (16) as well as Figure 4 of Reference[19].

d_{od}	Energy [eV]
5	-1.4571
4	-1.4567

b. Benchmark and validation

Among the first findings in SABRE was that Crabtree's catalyst $[Ir(COD)(PCy_3)]BF_4$ (Cy = cyclohexyl) (**1**) (see Fig. **S1**) which is transformed in-situ into the catalytically active dihydride tris-pyridine species $[Ir(H)_2(Pyr)_3(PCy_3)]^+$ (Pyr = Pyridine) (**1a**). We validated the accuracy of the chosen level of theory for geometric quantities first. To that end we performed a comparison between experimental periodic

structures obtained from X-ray data of $[Ir(H)_2(Pyr)_3(PCy_3)]BF_4$ (Pyr = Pyridine) and a geometry relaxation (also using periodic boundary conditions) using PBE+TS with tier2 basis set in FHI-aims.

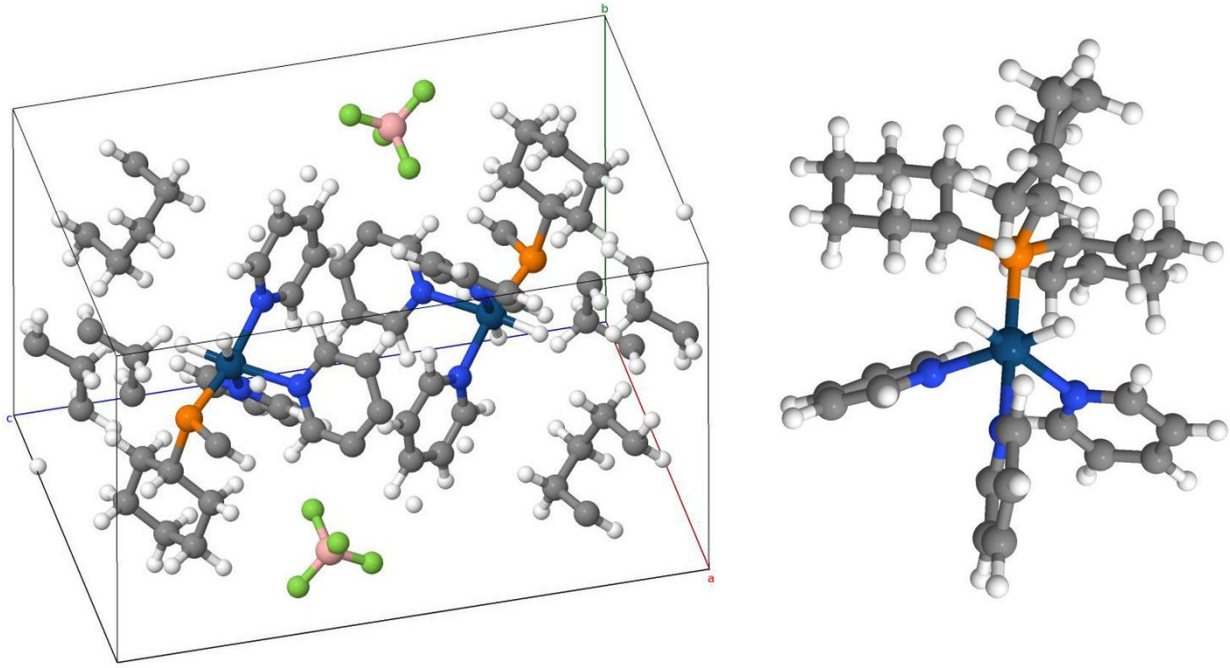

	a (Å)	*b (Å)*	*c (Å)*	*α (°)*	*β (°)*	*γ (°)*
PBE+TS	*9.871*	*10.197*	*17.646*	*94.1*	*96.2*	*110.7*
XRD[20]	*9.923*	*10.382*	*18.008*	*95.6*	*96.4*	*111.0*

Figure S1: Unit cell of the periodic structure of $[Ir(H)_2(Pyr)_3(PCy_3)]BF_4$ (left) and molecular complex $[Ir(H)_2(Pyr)_3(PCy_3)]^+$ (right) derived by considering only one formula unit of the periodic structure (without the BF_4^- counterions). The relaxed (PBE+TS) unit cell parameters compare to the XRD-derived values as shown in the table below. The agreement is close (2% or better), comparable to other uses of the same methodology for complex crystal structures, e.g., organic-inorganic hybrid crystals,[21, 22] in the literature.

In Figure S1 we show the result of the structure relaxation using PBE+TS and tier 2 basis sets. We compare the theoretical bond lengths found in the periodic structure of $[Ir(H)_2(Pyr)_3(PCy_3)]BF_4$ to experimental data. The unit cell contains two formula units of the $[Ir(H)_2(Pyr)_3(PCy_3)]^+$ complex. The exhaustive list is presented as table S5, a concise synopsis of the results is presented in table S4, where maximum error, mean absolute error and as well as standard deviation of bond lengths are compared. Note that the C-H bond lengths were fixed to 0.93 Å[23] in the experimental XRD refinement of Ref.[20] (Adrian C. Whitwood, private communication, 2019) and can therefore not be compared to the computational values, which reflect fully relaxed bond length values. In contrast, all bond lengths that were fully optimized both in experiment and theory agree closely.

Table S4 Synopsis of the results of the bond length comparison presented in Table S5. The standard deviation is defined as $\sigma = \sqrt{\frac{1}{N-1}\sum_{i=1}^{N}(x_i - \bar{x})^2}$ **, where *N* is the number of distances considered,** $x_i = d_i^{exp} - d_i^{theor}$ **, where** d_i^{exp} **is an experimental bond distance,** d_i^{theor} **is the corresponding calculated**

bond distance, and $\bar{x}$ is the average over all x_i. Note that the C-H bond lengths were fixed to 0.93 Å in the experimental XRD refinement[20, 23] and can therefore not be compared to the computational values, which reflect fully relaxed bond length values.

	Ir-N bonds	C-C bonds	C-H bonds	C-N bonds
Maximum error	0.0096 Å	0.0285 Å	0.1394 Å	0.0184 Å
Mean absolute error	0.0050 Å	0.0060 Å	0.1179 Å	0.0053 Å
Standard deviation	0.0041 Å	0.0076 Å	0.0131 Å	0.0058 Å

Table S5 Comparison of experimental and theoretical bond lengths in the periodic structure of $[Ir(H)_2(Pyr)_3(PCy_3)]BF_4$ using the PBE+TS level of theory and structure relaxation with the FHI-aims tier2 basis set. Bonds associated with atoms close to Iridium have the best agreement with experiment. Note that the C-H bond lengths were fixed to 0.93 Å in the experimental XRD refinement[20, 23] and can therefore not be compared to the computational values, which reflect fully relaxed bond length values.

		Distance, Å		
Atom 1	Atom 2	Experimental	Calculated	Absolute difference, Å
C8	C7	1.530651	1.5320742	0.001423
C9	C8	1.52798	1.5255792	0.002401
C10	C9	1.5268823	1.5269591	7.68E-05
C11	C10	1.530769	1.5326353	0.001866
C12	C7	1.5352157	1.5371894	0.001974
C12	C11	1.5472645	1.5384469	0.008818
C17	C16	1.5324448	1.5322238	0.000221
C18	C17	1.5376749	1.5354335	0.002241
C20	C19	1.3789754	1.3895522	0.010577
C21	C20	1.3851836	1.3923148	0.007131
C22	C21	1.386379	1.3908994	0.00452
C23	C22	1.3798811	1.3876511	0.00777
C25	C24	1.393684	1.3913983	0.002286
C26	C25	1.3775615	1.3925359	0.014974
C27	C26	1.3830091	1.3940248	0.011016
C28	C27	1.3856999	1.3880184	0.002318
C30	C29	1.3811597	1.388758	0.007598
C31	C30	1.3723245	1.3933392	0.021015
C33	C31	1.3633097	1.3916506	0.028341
C33	C32	1.3778028	1.3855554	0.007753
H34	C33	0.95048124	1.0857615	0.13528
H35	C32	0.94992393	1.0837675	0.133844
H36	C30	0.94931453	1.0876182	0.138304
H37	C31	0.95062494	1.0888366	0.138212
H38	C28	0.9498784	1.0864989	0.136621
H39	C29	0.9505268	1.0864323	0.135906

H40	C26	0.9493922	1.0882806	0.138888
H41	C27	0.9504502	1.0877148	0.137265
H42	C24	0.9504114	1.0859745	0.135563
H43	C25	0.94900876	1.0883982	0.139389
H44	C22	0.94994503	1.0870717	0.137127
H45	C23	0.9505284	1.0845433	0.134015
H48	C18	1.0007445	1.1048522	0.104108
H49	C19	0.9503667	1.0870075	0.136641
H50	C17	0.9894902	1.0968673	0.107377
H51	C17	0.99027663	1.1005701	0.110293
H54	C16	0.98942363	1.1026164	0.113193
H60	C12	1.000296	1.1026115	0.102316
H61	C11	0.9896426	1.0996801	0.110038
H62	C11	0.9900963	1.0980885	0.107992
H63	C10	0.9896697	1.0980076	0.108338
H64	C10	0.98959756	1.1025678	0.11297
H65	C9	0.9895037	1.1030235	0.11352
H66	C8	0.99017835	1.0971313	0.106953
H67	C9	0.99069035	1.0974722	0.106782
H68	C8	0.9901866	1.1037956	0.113609
H69	C7	0.98955095	1.0999519	0.110401
H70	C7	0.99030304	1.0987967	0.108494
H72	C6	0.99985933	1.103345	0.103486
N84	C32	1.3516445	1.3548028	0.003158
N85	C24	1.3464149	1.3509139	0.004499
N85	C28	1.3499315	1.3543807	0.004449
N86	C19	1.3552834	1.3522661	0.003017
N86	C23	1.3488213	1.3528872	0.004066
P87	C6	1.8604808	1.8772328	0.016752
P87	C12	1.8548868	1.8750621	0.020175
P87	C18	1.8696877	1.8842024	0.014515
Ir93	H82	1.5248421	1.5917895	0.066947
Ir93	H83	1.4822094	1.5832899	0.101081
Ir93	N84	2.1435943	2.1531923	0.009598
Ir93	N85	2.2160332	2.2165232	0.00049
Ir93	N86	2.2104962	2.2156096	0.005113
Ir93	P87	2.2429743	2.2588267	0.015852
C95	C94	1.5347363	1.5361127	0.001376
C96	C95	1.5247221	1.5314409	0.006719
C97	C96	1.5246669	1.5271133	0.002446
C98	C97	1.5340117	1.5315272	0.002485
C101	C100	1.5305866	1.5321032	0.001517
C102	C101	1.5280114	1.5254962	0.002515
C103	C102	1.5270519	1.5270128	3.91E-05
C104	C103	1.5306792	1.5326629	0.001984
C105	C100	1.5352163	1.5371895	0.001973
C105	C104	1.5472647	1.5384473	0.008817
C107	C106	1.5312545	1.5320477	0.000793

C108	C107	1.5266216	1.5302105	0.003589
C113	C112	1.3789756	1.3895527	0.010577
C114	C113	1.3852341	1.3922623	0.007028
C115	C114	1.3863786	1.3908995	0.004521
C116	C115	1.3799162	1.387651	0.007735
C118	C117	1.3936067	1.3913566	0.00225
C119	C118	1.3775353	1.3925297	0.014994
C120	C119	1.3829597	1.3939872	0.011028
C121	C120	1.3856999	1.3880631	0.002363
C123	C122	1.3812047	1.3886917	0.007487
C124	C123	1.3723435	1.3933228	0.020979
C126	C124	1.3631799	1.3916864	0.028507
C126	C125	1.3778698	1.3854457	0.007576
H127	C126	0.9504809	1.0857964	0.135316
H128	C125	0.949924	1.0837672	0.133843
H129	C123	0.9493137	1.0876999	0.138386
H130	C124	0.95057774	1.0888351	0.138257
H131	C121	0.9498779	1.0866172	0.136739
H132	C122	0.9504373	1.086432	0.135995
H133	C119	0.9494681	1.0883152	0.138847
H134	C120	0.9504808	1.0877148	0.137234
H135	C117	0.9504642	1.0860586	0.135594
H136	C118	0.9490095	1.0883613	0.139352
H137	C115	0.95003116	1.0870717	0.137041
H138	C116	0.95045316	1.0845869	0.134134
H142	C112	0.95031834	1.0870575	0.136739
H146	C108	0.99039316	1.099766	0.109373
H148	C108	0.9893346	1.101815	0.11248
H149	C107	0.9900765	1.1023656	0.112289
H150	C107	0.9903269	1.100134	0.109807
H151	C106	0.989633	1.1007886	0.111156
H152	C106	0.98999166	1.0938039	0.103812
H153	C105	1.0003793	1.1026686	0.102289
H154	C104	0.9896429	1.0997535	0.110111
H155	C104	0.9900128	1.0980093	0.107997
H156	C103	0.98957115	1.0979886	0.108417
H157	C103	0.9895595	1.1024827	0.112923
H158	C102	0.9894923	1.1030791	0.113587
H159	C101	0.9902517	1.0971318	0.10688
H160	C102	0.9906912	1.0974499	0.106759
H161	C101	0.99018633	1.1037724	0.113586
H162	C100	0.9895501	1.0999513	0.110401
H163	C100	0.99033713	1.0987763	0.108439
H164	C98	0.98989516	1.1021744	0.112279
H166	C98	0.9892722	1.0949287	0.105657
H167	C97	0.9896607	1.100961	0.1113
H168	C97	0.99039066	1.1029596	0.112569
H169	C96	0.9906727	1.0966203	0.105948

H170	C96	0.9907734	1.1033107	0.112537
H171	C95	0.9906518	1.1023278	0.111676
H172	C95	0.9895552	1.0999342	0.110379
H174	C94	0.98939764	1.0984722	0.109075
N177	C122	1.3326757	1.3510835	0.018408
N177	C125	1.351575	1.3548087	0.003234
N178	C117	1.3463421	1.3509134	0.004571
N178	C121	1.3499315	1.35426	0.004328
N179	C112	1.3552665	1.3523238	0.002943
P180	C105	1.8549597	1.8750619	0.020102
Ir186	H175	1.5247836	1.5917194	0.066936
Ir186	H176	1.4821151	1.5832902	0.101175
Ir186	N177	2.1436605	2.1531675	0.009507
Ir186	N178	2.216156	2.216523	0.000367
Ir186	N179	2.210548	2.2156966	0.005149
Ir186	P180	2.2429743	2.2587514	0.015777
C1	C6	1.5363721	1.5381867	0.001815
C1	H80	0.9894048	1.0952778	0.105873
C2	C1	1.5347642	1.5360495	0.001285
C3	C2	1.5248146	1.5314409	0.006626
C4	C3	1.5245708	1.527113	0.002542
C5	C6	1.5385642	1.535671	0.002893
C5	C4	1.5340122	1.5314348	0.002577
C13	C18	1.5358702	1.5336901	0.00218
C14	C13	1.531331	1.5322595	0.000929
C15	C16	1.5215708	1.5323185	0.010748
C15	C14	1.5266012	1.5300859	0.003485
H46	C20	0.9492031	1.0876293	0.138426
H47	C21	0.949908	1.0843836	0.134476
H52	C16	0.9896243	1.1011136	0.111489
H53	C15	0.99045974	1.0999047	0.109445
H55	C15	0.98924935	1.1018888	0.112639
H56	C14	0.98998874	1.1023735	0.112385
H57	C14	0.99037	1.1000499	0.10968
H58	C13	0.98963314	1.100697	0.111064
H59	C13	0.9899916	1.0938916	0.1039
H71	C5	0.98976105	1.1020961	0.112335
H73	C5	0.9893693	1.0948408	0.105472
H74	C4	0.9896606	1.1009532	0.111293
H75	C4	0.9904477	1.1030682	0.112621
H76	C3	0.9906925	1.0967629	0.10607
H77	C3	0.9907503	1.1033725	0.112622
H78	C2	0.9907002	1.1022977	0.111598
H79	C2	0.9895552	1.0999405	0.110385
H81	C1	0.98939824	1.0984527	0.109054
C99	C94	1.5363722	1.5383646	0.001992
C99	C98	1.5385642	1.5355052	0.003059
C109	C108	1.5215364	1.5324639	0.010928

C109	H145	0.9896196	1.1010251	0.111406
C110	C109	1.5324448	1.5321747	0.00027
C111	C106	1.5359092	1.5336839	0.002225
C111	C110	1.5376648	1.5353292	0.002336
C113	H139	0.9491571	1.0875636	0.138407
C114	H140	0.9499077	1.0844247	0.134517
H141	C111	1.0006518	1.1049458	0.104294
H143	C110	0.9895276	1.0967481	0.107221
H144	C110	0.9902768	1.1005703	0.110294
H147	C109	0.98944044	1.1026679	0.113227
H165	C99	0.99977934	1.1034801	0.103701
H173	C94	0.98935056	1.095118	0.105767
P180	C99	1.8604522	1.8772084	0.016756
P180	C111	1.8697284	1.8842863	0.014558

We now compare the experimental unit cell geometry to the geometry of the $[Ir(H)_2(Pyr)_3(PCy_3)]^+$ complex obtained by relaxing the isolated system (Fig. S1, right). The purpose is to show that the bond distances change very little when going from periodic to non-periodic system and that the good agreement with experiment, as shown in Tables S4 and S5, is likely transferable to the molecules used in this study. Table S6 is a synopsis comparing maximum and mean absolute errors and standard deviation between the experimental periodic and the calculated non-periodic systems. The exhaustive list of bond distances is shown in Table S7.

Table S6 Synopsis of the results from Table S7. Maximum, mean absolute error and standard deviation of bond lengths between the theoretical $[Ir(H)_2(Pyr)_3(PCy_3)]^+$ molecule (PBE+TS, tier 2 basis set) and the experimental periodic structure The standard deviation is defined as $\sigma = \sqrt{\frac{1}{N-1}\sum_{i=1}^{N}(x_i - \bar{x})^2}$ **, where *N* is the number of distances considered,** $x_i = d_i^{exp} - d_i^{theor}$ **, where** d_i^{exp} **is an experimental bond distance,** d_i^{theor} **is the corresponding calculated bond distance, and** $\bar{x}$ **is the average over all** x_i**. Note that the C-H bond lengths were fixed to 0.93 Å in the experimental XRD refinement[20, 23] and can therefore not be compared to the computational values, which reflect fully relaxed bond length values.**

	Ir-N bonds	C-C bonds	C-H bonds	C-N bonds
Maximum error	0.0169 Å	0.0314 Å	0.1397 Å	0.0189 Å
Mean absolute error	0.0096 Å	0.0073 Å	0.1189 Å	0.0059 Å
Standard deviation	0.0064 Å	0.0072 Å	0.0135 Å	0.0074 Å

Table S7 Comparison of bond lengths between the theoretical $[Ir(H)_2(Pyr)_3(PCy_3)]^+$ molecule (PBE+TS, tier 2 basis set) and the experimental periodic structure. Note that the C-H bond lengths were fixed to 0.93 Å in the experimental XRD refinement[20, 23] and can therefore not be compared to the computational values, which reflect fully relaxed bond length values.

		Distance, Å		
Atom 1	Atom 2	Experimental	Calculated	Absolute difference, Å

Ir82	N85	2.1502943	2.1435943	0.0067
N85	C9	1.3515714	1.3326348	0.018937
C9	C7	1.3902243	1.3811597	0.009065
C7	C5	1.3927441	1.3723245	0.02042
C5	C3	1.3947259	1.3633097	0.031416
C3	C1	1.3884838	1.3778028	0.010681
C1	N85	1.354299	1.3516445	0.002655
C9	H10	1.0878944	0.9505268	0.137368
C7	H8	1.088576	0.94931453	0.139261
C5	H6	1.089026	0.95062494	0.138401
C3	H4	1.0884813	0.95048124	0.138
C1	H2	1.0869839	0.94992393	0.13706
Ir82	N86	2.2328978	2.2160332	0.016865
N86	C19	1.3498614	1.3464149	0.003446
C19	C17	1.3906088	1.393684	0.003075
C17	C15	1.393093	1.3775615	0.015531
C15	C13	1.39353	1.3830091	0.010521
C13	C11	1.390122	1.3856999	0.004422
C11	N86	1.352609	1.3499315	0.002677
C19	H20	1.0881885	0.9504114	0.137777
C17	H18	1.0886824	0.94900876	0.139674
C15	H16	1.0890508	0.9493922	0.139659
C13	H14	1.0885752	0.9504502	0.138125
C11	H12	1.087527	0.9498784	0.137649
Ir82	N87	2.215596	2.2104962	0.0051
N87	C21	1.3534802	1.3488213	0.004659
C21	C23	1.3896275	1.3798811	0.009746
C23	C25	1.3938025	1.386379	0.007424
C25	C27	1.3931648	1.3851836	0.007981
C27	C29	1.3903133	1.3789754	0.011338
C29	N87	1.3520924	1.3552834	0.003191
C21	H22	1.0880502	0.9505284	0.137522
C23	H24	1.0885264	0.94994503	0.138581
C25	H26	1.0889671	0.949908	0.139059
C27	H28	1.0887014	0.9492031	0.139498
C29	H30	1.0881515	0.9503667	0.137785
P88	C65	1.876243	1.8604808	0.015762
C65	C67	1.5403095	1.5385642	0.001745
C67	C70	1.5366845	1.5340122	0.002672
C70	C73	1.5325035	1.5245708	0.007933
C73	C76	1.5326344	1.5248146	0.00782
C76	C79	1.5335318	1.5347642	0.001232
C79	C65	1.5393647	1.5363721	0.002993
C67	H69	1.0982211	0.9893693	0.108852
C67	H68	1.0996115	0.98976105	0.10985
C70	H72	1.104032	0.9904477	0.113584
C70	H71	1.0995797	0.9896606	0.109919
C73	H75	1.0994381	0.9906925	0.108746

C73	H74	1.1029966	0.9907503	0.112246
C76	H77	1.1039749	0.9907002	0.113275
C76	H78	1.0997901	0.9895552	0.110235
C79	H80	1.0973781	0.9894048	0.107973
C79	H81	1.1013341	0.98939824	0.111936
C65	H66	1.1037654	0.99985933	0.103906
P88	C48	1.8752105	1.8548868	0.020324
C48	C50	1.5397974	1.5472645	0.007467
C50	C53	1.5342249	1.530769	0.003456
C53	C56	1.5305094	1.5268823	0.003627
C56	C59	1.5305246	1.52798	0.002545
C59	C62	1.5338433	1.530651	0.003192
C62	C48	1.5393277	1.5352157	0.004112
C50	H52	1.0985879	0.9900963	0.108492
C50	H51	1.0984904	0.9896426	0.108848
C53	H55	1.0997148	0.9896697	0.110045
C53	H54	1.1029787	0.98959756	0.113381
C56	H57	1.1044728	0.9895037	0.114969
C56	H58	1.0991322	0.99069035	0.108442
C59	H60	1.0999935	0.99017835	0.109815
C59	H61	1.1028306	0.9901866	0.112644
C62	H63	1.0996208	0.98955095	0.11007
C62	H64	1.100255	0.99030304	0.109952
C48	H49	1.1026697	1.000296	0.102374
P88	C31	1.8761292	1.8697284	0.006401
C31	C33	1.5394292	1.5376648	0.001764
C33	C36	1.5349053	1.5324448	0.00246
C36	C39	1.5316653	1.5215364	0.010129
C39	C42	1.5311345	1.5266216	0.004513
C42	C45	1.5354599	1.5312545	0.004205
C45	C31	1.5401442	1.5359092	0.004235
C33	H34	1.100615	0.9895276	0.111087
C33	H35	1.0965179	0.9902768	0.106241
C36	H37	1.0998304	0.98944044	0.11039
C36	H38	1.1036011	0.9896196	0.113982
C39	H41	1.1032556	0.99039316	0.112862
C39	H40	1.0993583	0.9893346	0.110024
C42	H44	1.0996379	0.9900765	0.109561
C42	H43	1.1034403	0.9903269	0.113113
C45	H47	1.1008606	0.98999166	0.110869
C45	H46	1.0985909	0.989633	0.108958
C31	H32	1.1053195	1.0006518	0.104668
Ir82	H84	1.5824903	1.5247718	0.057719
Ir82	H83	1.5884556	1.4822097	0.106246
Ir82	P88	2.2830832	2.2429743	0.040109

c. The Phox dihydride

The Phox catalyst **(3,3a)** is a variant of Crabtree's catalyst with a bidentate ligand.

We first consider all different coordination patterns of hydrides possible in an octahedral $[Ir(H)_2(MP)_2(Phox)]^+$ (MP = 2-methylpyridine) complex. Initial geometry guesses are created from X-ray data of similar compounds, such as $[Ir(H)_2(Pyr)_3(PCy_3)]BF_4$ (**1a**) shown in Fig S1. Structure relaxation is carried out in FHI aims using a full set of PBE+TS, PBE+Sol and a comparison with the M06-x functional. Converged geometries and energy differences between several different hydride coordination modes of the Phox catalyst (**3a**) after structure relaxation are compared in Figure S2.

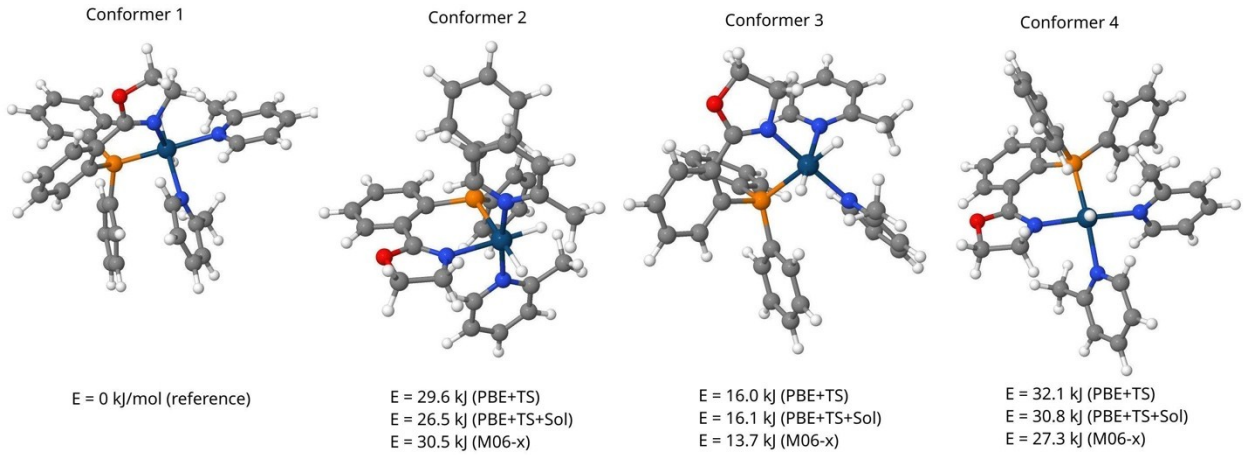

Figure S2: Comparison of the DFT energies of coordination patterns for the dihydride-bis substrate complex considering Oxazoline-N coordination. We compare PBE+TS, PBE+TS with implicit solvent correction, and M06 functionals. The most stable configuration identified is afforded by the two hydrides coordinating trans-to-substrate and trans*-to-oxazoline, consistent with the expected catalyst structure and NMR observations. This structure is labelled as conformer 1 throughout the supporting information and is denoted (3a) in the text of the main paper (Figure 2A). Note that different viewing orientations of the structures are chosen to enable visualization of the main bonding features that is complementary (i.e., provides additional visual information) to the views shown in the main text. The second hydride H atom coordinated to Ir in "conformer 4" is behind the Ir atom, i.e., at 180° compared to its visible counterpart.*

The most stable structure (0 kJ/mol) considered is the coordination pattern with hydride coordination trans-to nitrogen, instead of phosphorous. This is consistent with the literature concerning bonding preferences of hydride complexes in metal hydrides[24] and the geometry found for the dihydride of Crabtree's catalyst discussed previously.

To gain further insight into the bonding of the catalytically active species we considered different conformers of the most stable hydride coordination patterns with respect to ligand rotations as shown in Figure S3.

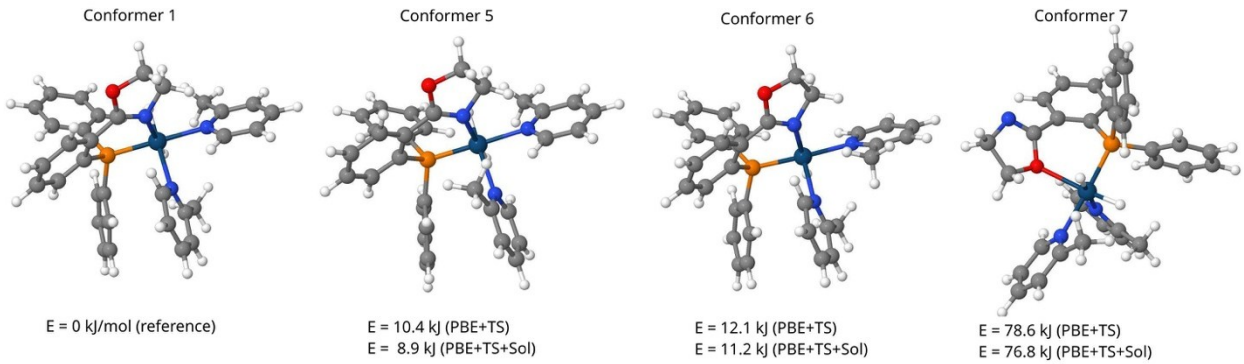

Figure S3: Comparison of conformer energies after geometry relaxation. We consider complexes using PBE+TS and PBE+TS with solvent correction. The lowest energy structure, conformer 1, is shown on the left. For conformer 5 the trans-to-H 2-methylpyridine has been rotated by 180°, conformer 6 is obtained by 180° rotation of the trans-to-P 2-methylpyridine. Conformer 7 considers the oxygen bound oxazoline moiety.

We find conformer 1 to be the most stable structure. Rotations of the 2-methylpyridine affords slightly less favourable geometries, whereas oxygen coordination of the oxazoline moiety is found to be significantly less favourable.

For completeness we also considered possible methanol adducts to the complex, with the geometries obtained after structure relaxation shown in Figure S4. Using the energy of the different adducts, our reference species (Conformer 1) and the energy of the fragments 2-methylpyridine, methanol (see Table S8a), we can calculate the energy difference associated with replacement of nitrogen bearing ligands by methanol (see Table S8b).

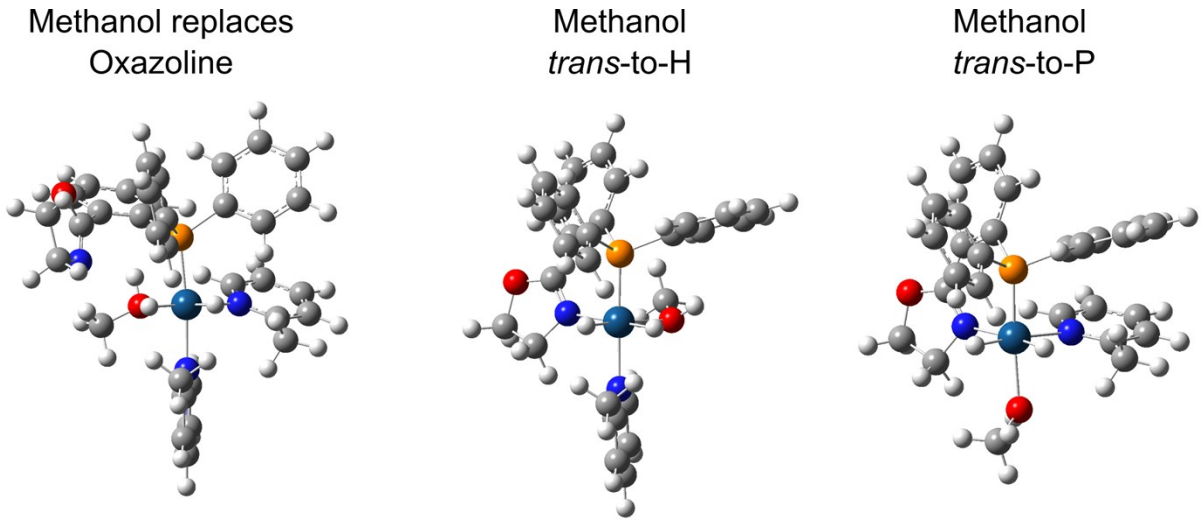

Figure S4: Converged geometries of three different methanol adducts (called adduct A2, A3, and A4 from left to right and in Tables S8a and S8b below) to the dihydride using PBE+TS and FHI-aims tier 2 basis sets. We omit naming any adduct "A1" to avoid confusion with "conformer 1", which serves as the reference species in our calculations.

Table S8a. Converged energies of fragments and complexes related to adducts A2, A3, and A4 (PBE+TS, tight settings, FHI-aims)

Species	Molecule/Fragment	Energy PBE+TS [eV]	Energy PBE+TS+Solvent correction [eV]
1	Conformer 1	-551927.783	-551929.474
A2	Methanol replaces Oxazoline	-555077.343	-555079.065
A3	Methanol trans-to-H	-547251.799	-547253.674
A4	Methanol trans-to-P	-547251.937	-547253.671
F1	2-methylpyridine (2M)	-7824.944	-7825.073
F2	Methanol (M)	-3149.808	-3149.999

Table S8b. Relationship between reference species and fragments and bonding energy differences. We consider methanol against 2-methylpyridine coordination (A3, A4) as well as displacement of the oxazoline moiety by a methanol molecule (A2).

Relation between Species	Energy PBE+TS [eV]	Difference to reference [eV] ([kJ/mol])	Energy PBE+TS+Sol [eV]	Difference to reference [eV] ([kJ/mol])
1 (reference)	-551927.783	0	-551929.474	0
A2 - F2	-551927.535	0.248 (23.93)	-551929.066	0.408 (39.4)
A3 + F1 - F2	-551926.936	0.847 (83.94)	-551928.748	0.726 (70.0)
A4 + F1 - F2	-551927.074	0.709 (68.41)	-551928.745	0.729 (70.3)

The results of the calculations (including and excluding solvent correction) are qualitatively identical. Considering the solvent adducts, theory predicts *trans*-to-P coordination (A4) to be energetically somewhat similar to *trans*-to-H coordination (A3, especially when including the implicit solvent correction). However, both are energetically rather unfavorable. Loss of the non-aromatic oxazoline moiety and replacement by methanol (A2) is less dramatic than replacement of aromatic 2-methylpyridine.

In the experimental studies we found the Phox catalyst (**3a**) to perform well for 2-substituted, but not for 2,6-disubstituted substrates with a large degree of sterical hindrance. We derived a structural analogue of the 2,6-dimethylpyridine adduct and compare structures and energies of our reference geometry (conformer 1) and the new species, called adduct A5 and shown in Fig. S5.

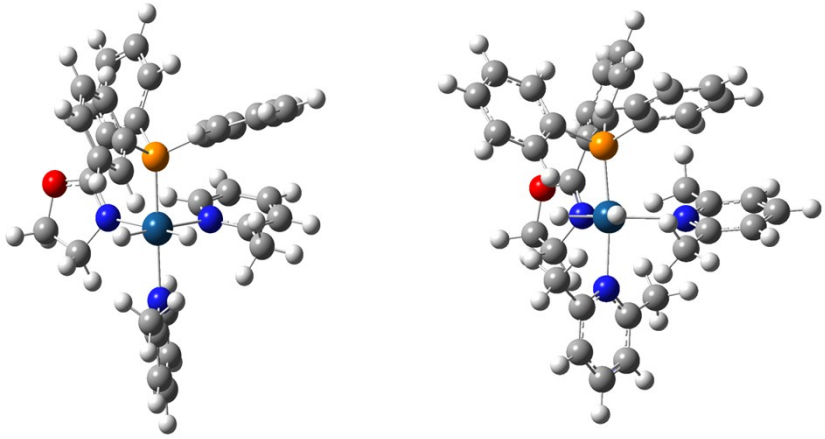

Figure S5: Conformer 1 and a bis-2,6-dimethylpridine adduct (called adduct A5) constructed by analogy after geometry relaxation.

Table S9 Comparison of energies of Conformer 1 and the 2,6-dimethylpyridine analogue, adduct A5. We show the energy difference as well as the total energies of individual fragments, calculated using FHI-aims tight settings and comparing DFT-PBE+TS and DFT-PBE+TS+Sol, for reference.

	Quantity	Energy, PBE+TS [eV]	Energy, PBE+TS+Sol [eV]
1+2F3 -> A5+2F1	Energy of reaction	0.541	0.496
A5	E_{tot}, 2,6-dimethylpyridine adduct	-554066.462	-554068.158
F3	E_{tot}, 2,6-dimethylpyridine	-8894.554	-8894.663
F1	E_{tot}, 2-methylpyridine	-7824.944	-7825.073
1	E_{tot}, Conformer 1	-551927.783	-551929.474

We use Table S9 to estimate the additional energy required to bind 2,6-dimethylpyridine vs. 2-methylpyridine, which amounts to 0.54 eV (0.5 eV) using DFT-PBE+TS and DFT-PBE+TS+Sol, i.e., without and with including a solvent model. The large and unfavorable energy change when substituting 2,6-dimethylpyridine for 2-methylpyridine could be due, partially, to strain or electrostatic effects. The energy change of approximately 0.5 eV (see Table S9) is a significant barrier for di-substituted pyridine rings. It is hence not surprising that we find no enhancements for 2,6-dimethylpyridine in our SABRE study (see Table 1 of the main text).

d. Strain effects

To see if strain effects are relevant, we compare the bond length and bond angles within the complexes and the substrates (for calculated geometries using DFT-PBE+TS). First, we consider the complexes (conformer 1 and adduct A5), which differ only in the ligands, 2-methylpyridine in conformer 1 vs. 2,6 dimethylpyridine in adduct A5. In Tables S10 and S11, we compare the local geometry near the transition

metal site, which can act as a hinge to alter the extended geometry of the complex. Indeed, the most significant difference is the change in N-Ir-P angle (Table S11), which deviates significantly more from 180° in adduct A5 vs. conformer 1, as a consequence of needing to accommodate the larger 2,6 dimethylpyridine ligand. This local change also displaces the more distant parts of the complex compared to an unstrained conformation. This is important because in complex systems, strain can be a combination of a large amount of small local changes that add up.

Table S10 Comparison of bond lengths in conformer 1 and adduct A5. Notation for the nitrogen atoms is as follow: N1 – part of the 2,6-dimethylpyridine adduct, opposite to the P atom in reference to Ir; N2 - part of the 2,6-dimethylpyridine adduct, forms a right angle with Ir and P; N3 – part of the oxazoline moiety.

Atom 1	Atom 2	Conformer 1	Adduct A5
Ir	P	0.222 nm	0.221 nm
Ir	N1	0.216 nm	0.223 nm
Ir	N2	0.225 nm	0.238 nm
Ir	N3	0.218 nm	0.221 nm

Table S11 Comparison of bond angles in conformer 1 and adduct A5. Notation for the nitrogen atoms is the same as in Table S12.

Atom 1	Atom 2	Atom3	Conformer 1	Adduct A5
N1	Ir	P	176.2°	170.5°
N2	Ir	P	93.3°	95.6°
N3	Ir	P	90.6°	90.5°
N1	Ir	N2	88.4°	91.1°
N1	Ir	N3	92.7°	93.4°
H	Ir	H	86.3°	88.5°

In contrast to the complex, the strain in the ligands appears to be relatively small as can be seen in tables S12 and S13. As seen from Table S12, the difference between bond lengths is very small for both the 2-methylpyridine and 2,6-dimethylpyridine molecules. The difference in angles is more noticeable (Table S13) but still small and leads us to surmise that strain is largely accommodated by the remainder of the complex, not the adduct.

Table S12 Bond lengths in bound and free molecules. Note that virtually no bond length differences exist for bound ligands irrespective of trans-to H or trans to-P coordination.

	Atom1[a]	Atom 2[a]	Bound species bond length [nm]	Free species Bond length [nm]	Difference [nm]
2-Methylpyridine	N1	C2	0.136	0.135	0.001
	N1	C6	0.136	0.134	0.002
	C2	C3	0.140	0.140	-
	C5	C6	0.139	0.140	0.001
	C3	C4	0.139	0.139	-
	C4	C5	0.139	0.139	-
	C2	C7	0.149	0.150	0.001
2,6-Dimethylpyridine	N1	C2	0.137	0.134	0.003
	N1	C6	0.137	0.134	0.003
	C2	C3	0.140	0.140	-
	C5	C6	0.140	0.140	-
	C3	C4	0.139	0.139	-
	C4	C5	0.139	0.139	-
	C2	C8	0.150	0.150	-
	C6	C9	0.150	0.150	-

a) Heterocycle nomenclature for labels, start counting at 1 for heteroatom (N), ring-carbons C2 - C6, C7 and C8 = methyl.

Table S13 Bond angles in bound and free molecules. We compare average bond angles differences between the two sites with free material.

	Atom1[a]	Atom 2[a]	Atom 3[a]	Bound species bond angle [°]	Free species bond angle [°]	Difference [°]
2-Methylpyridine	C6	N1	C2	118	118.1	0.1
	C7	C2	N1	120	116.4	3.6
	C3	C4	C5	118.1	118.8	0.7
	C7	C2	C3	119.7	121.7	2.0
2,6-Dimethylpyridine	C6	N1	C2	117.4	119.2	-1.8
	C3	C2	N1	121.4	116.3	+5.1
	C3	C4	C5	117.6	119	-1.4
	C7	C2	C3	116.8	121.7	-4.9

a) Labels as in Tables S12.

e. Local transition metal center coordination geometry

For a final quality assessment of our DFT calculations we compare structural parameters from theory (PBE+TS, FHI aims tier 2 basis sets) for conformer 1 (Figure S1, left) and X-ray data of $[Ir(H)_2(Pyr)_3(PCy_3)]^+$ (Pyr = Pyridine, Cy = cyclohexyl, (H)[20], the active species in SABRE obtained with the canonical Crabtree-catalyst. Of particular relevance is the first coordination sphere around the central Ir(III) particle. In both complexes the coordination sphere contains two Ir-H bonds, one Ir-P, and three Ir-N bonds. Other parameters of interest are the distance between the hydrides as well as the H-Ir-H angle, which provides important information about the classical/non-classical nature of the dihydride.[24, 25] Due to structural differences beyond the first coordination sphere, only a comparison of C-C and C-N bond length in the

pyridine molecules is considered (note that the phosphine ligands have phenylgroups in $[Ir(H)_2(MP)_2(Phox)]^+$ and cyclohexyl groups in $[Ir(H)_2(Pyr)_3(PCy_3)]$). Tables S14 and S15 demonstrate that the relevant bond distances and angles are virtually unchanged between different structures. The DFT calculations point to a stable dihydride, where for third row transition metals H1-H2 distances larger than 200 pm and H1-M-H2 angles around 90° are considered characteristic of a fully classical hydride.[24, 26]

Table S14 Comparison of calculated and experimental bond length between the $[Ir(H)_2(Pyr)_3(PCy_3)]BF_4$ crystal, the $[Ir(H)_2(Pyr)_3(PCy_3)]^+$ complex and the $[Ir(H)_2(MP)_2(Phox)]^+$ complex. (MP = 2,6 dimethylpyridine)

		$[Ir(H)_2(Pyr)_3(PCy_3)]BF_4$		$[Ir(H)_2(Pyr)_3(PCy_3)]^+$	$[Ir(H)_2(MP)_2(Phox)]^+$
Atom 1	Atom 2	Experimental [nm]	Calculated [nm]	Calculated [nm]	Calculated [nm]
Ir 93	H 82	0.152	0.159	0.159	0.159
Ir 93	H 83	0.148	0.158	0.158	0.158
Ir 93	N 85	0.222	0.222	0.225	0.225
Ir 93	N 84	0.214	0.215	0.216	0.216
Ir 93	N 86	0.221	0.222	0.218	0.218
Ir 93	P 87	0.224	0.226	0.222	0.222
N 85	C 28	0.135	0.135	0.136	0.136
N 85	C 24	0.135	0.135	0.135	0.135
N 84	C 32	0.135	0.135	0.136	0.136
N 84	C 29	0.133	0.135	0.136	0.136

Table S15 Comparison of calculated and experimental bond angles between the $[Ir(H)_2(Pyr)_3(PCy_3)]BF_4$ crystal, the $[Ir(H)_2(Pyr)_3(PCy_3)]^+$ complex and the $[Ir(H)_2(MP)_2(Phox)]^+$ complex. (MP = 2,6 dimethylpyridine)

			$[Ir(H)_2(Pyr)_3(PCy_3)]BF_4$		$[Ir(H)_2(Pyr)_3(PCy_3)]^+$	$[Ir(H)_2(MP)_2(Phox)]^+$
Atom 1	Atom 2	Atom 3	Experiment [°]	Calculated [°]	Calculated [°]	Calculated [°]
H 82	Ir 93	H 83	92.7	88.3	86.3	86.3
P 87	Ir 93	N 84	168.6	164.9	176.2	176.2
N 85	Ir 93	N 86	97.5	95.3	96.5	96.5
N 85	Ir 93	N 84	84.6	88.1	88.4	88.4
H 82	Ir 93	N 86	175.8	174.7	171.1	171.1
H 83	Ir 93	N 85	171.9	173.4	178.4	178.4
H 82	Ir 93	N 84	92.5	89.6	89	89
P 87	Ir 93	H 83	82.6	80.1	87.5	87.5
C 28	N 85	C 24	117	117	118	118

3) Experimental procedure

For ^{1}H hyperpolarisation, a sample with a precatalyst concentration of c_{cat} = 2.6 mM and substrate concentration of c_{sub} = 50 mM was prepared using MeOH-d_4 as solvent. For hyperpolarisation of ^{1}H, the magnetic evolution field is adjusted by a small solenoid on the top of the NMR magnet. In ^{1}H hyperpolarisation, the sample is supplied with 160 standard cubic centimeters per minute (sccm) of *p*-H_2 gas (pressure 10 bar) for 30 s. Optimal evolution field is found to be B_{evo} = 140 – 150 G. For the PASADENA type experiments, a low flow of *para*-hydrogen (70 sccm) is constantly supplied at high magnetic field (8.45 T); detection utilizes 45° pulse excitation (16 scans, 7-second delay for H_2 exchange). For ^{15}N polarisation build-up, the sample is placed inside a solenoid coil inside a three-layer magnetic shield at a field of 0.66 µT. *Para*-H_2 is supplied at 200 sccm for 90 s. All data was acquired on a Bruker DX360 spectrometer.

Sample preparation

A small amount (between 1 and 3 mg, i.e., approximately the tip of a spatula) of PHOX catalyst was weighed and dissolved in an appropriately chosen volume MeOH-d_4 to yield a 2.6 mM solution of catalyst. To the bright red solution liquid substrates are added with an Eppendorf pipette; for solid substrates an appropriate volume of substrate solution (or neutralized solution for HCl salts) is added to the catalyst. The sample is transferred to a medium wall pressure NMR tube (Wilmad 524-PV-7), hydrogen flow is supplied with a capillary and adjusted with a needle valve.

The sample was characterized by ^{1}H NMR spectroscopy before H_2 exposure. The sample was then activated with 10 bars H_2 pressure and 1 h constant bubbling. The activation process is monitored by ^{1}H NMR, and catalyst activation was considered complete when peaks in the region δ = (- 14 to -16) ppm vanish (typically 15 - 30 minutes of low flow-rate *para*-H_2 bubbling). These peaks are associated with hydrides trans to COD (cyclooctadiene). These peaks disappear when the COD ligands are fully hydrogenated, which indicates the end of the catalyst activation period.
In order to validate the data of Table 1, especially for the data points where we report zero enhancements, we carefully followed the chemical shift change of the hydrides during activation as described.

^{1}H SABRE

For the ^{1}H SABRE experiments a small solenoid coil (12.3 G/V at R = 33 Ohm), placed on top of the NMR magnet, was used to vary the evolution field. For polarisation build-up the sample was placed in the middle of the coil at a desired evolution field (40 – 240 G) and *para*-hydrogen was bubbled through the solution with a flow rate of 120 sccm for 30 s. After the H_2-flow was stopped the sample was rapidly transferred to the magnet for detection. For polarisation dependence as function of the temperature the coil was immersed in a water bath at the field determined as optimal for the respective compound in room-temperature studies.

^{15}N SABRE-SHEATH

For SABRE-SHEATH experiments the sample is placed in a three-layer μ-metal shield equipped with a small solenoid coil as described previously.[27] An small magnetic field (typically 0.6 μT) was applied and *para*-hydrogen was supplied at 200 sccm for 90 s. Note that ^{15}N-polarisation shows strong dependence on hydrogen flow-rates and build-up time can be strongly substrate dependent.[28] To study the dependence of ^{15}N polarisation on the temperature a water bath is placed inside the shield.[29]

^{19}F SABRE-SHEATH

The procedure is identical to ^{1}H or ^{15}N SABRE experiments described before, however due to unknown optimal matching field for ^{19}F SABRE the magnetic field had to be varied over a wide range (0.1 μT - 10 mT). We found the highest signal intensity at 5.4 mT.

For all SABRE experiments enhancements are calculated as the ratio of peak areas between spectra from hyperpolarized and thermally polarized spins. All spectra are acquired on a Bruker DX 360 (8.45 T). All data was processed in Mnova 8.0.

4) Spectral data

2-Ethylpyridine

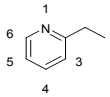

^{1}H NMR, 360 MHz, MeOH-d4, δ (ppm): 8.41 (1H, m), 7.75 (1H, m),7.32 (1H, m), 7.23 (1H, m), 2.80 (2H, q, *J* = 7.5 Hz), 1.28 (3H, t, *J* = 7.5 Hz).

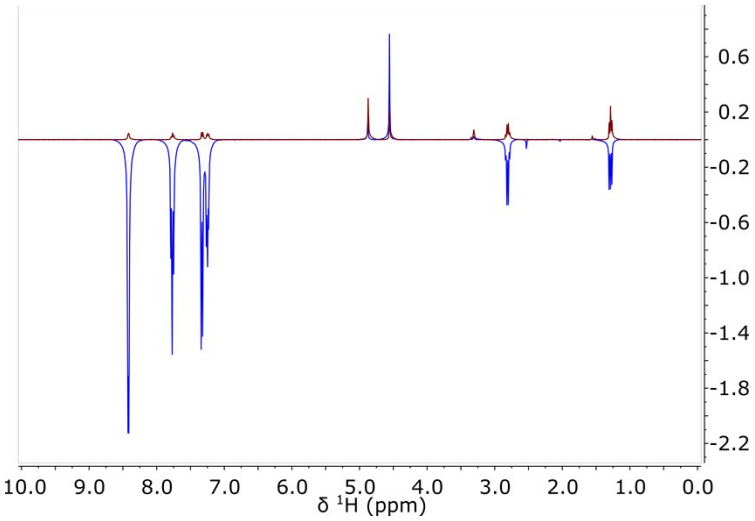

Figure S6: Comparison between a single scan ^{1}H spectrum of thermally polarized 2-ethylpyridine (red) and hyperpolarized spins (blue). The magnetic evolution field for the hyperpolarized experiment is 140 G, where maximum enhancement of aromatic protons is observed.

2-Methylpyridine

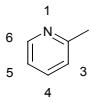

^{1}H NMR, 360 MHz, MeOH-d4, δ (ppm): 8.39 (m), 7.73 (m), 7.31 (m), 7.22 (m), 2.52 (s).

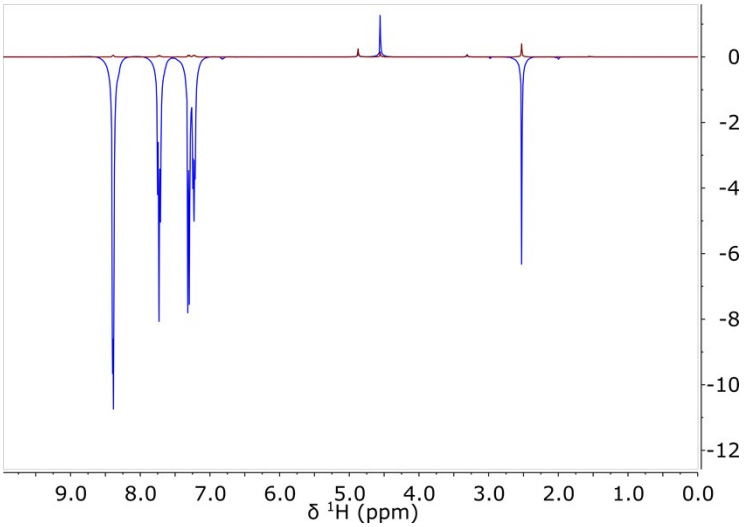

Figure S7: Comparison between a single scan ^{1}H spectrum of thermally polarized 2-methylpyridine (red) and hyperpolarized equivalent (blue). The magnetic evolution field is 140 G.

2-Fluoropyridine

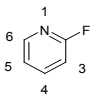

^{1}H NMR, 360 MHz, MeOH-d4, δ (ppm): 8.21 (1H, m), 7.96 (1H, m), 7.31 (1H, m), 7.08 (1H, m).

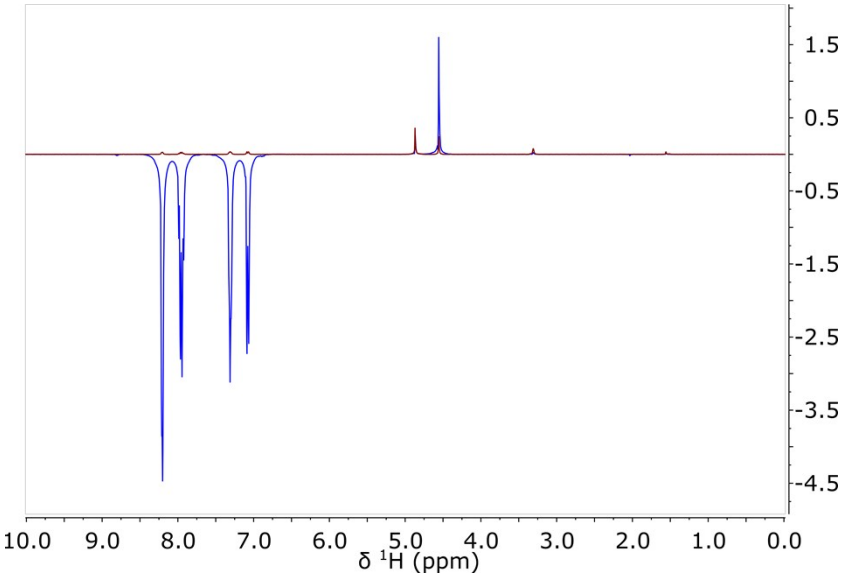

Figure S8: Comparison between a single scan ^{1}H spectrum of thermally polarized 2-fluoropyridine (red) and hyperpolarized equivalent (blue). The magnetic evolution field is 140 G.

4,5 Bis(hydroxymethyl)-2-methyl-3-pyridinol (Pyridoxine)

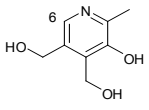

^{1}H NMR, 360 MHz, MeOH-d4, δ (ppm): 7.84 (1H, s), 4.95 (s), 4.89 (sb), 4.6 (s), 2.41 (3H, s).

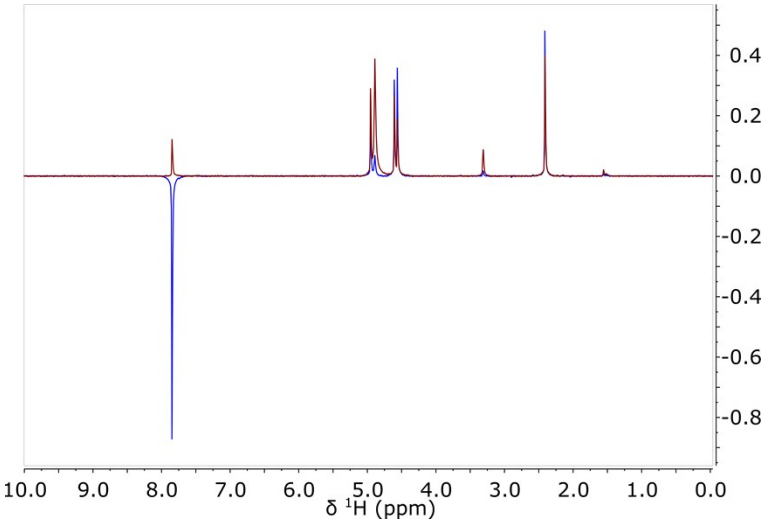

Figure S9: Comparison between a single scan ^{1}H spectrum of thermally polarized pyridoxine hydrochloride neutralized with 1eq. NaOD (red) and hyperpolarized trace (blue). Enhancements are mediocre, which is commonly observed using HCl salts as substrates. Evolution field is 140 G.

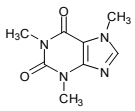

1,3,7-Trimethyl-3,7-dihydro-1H-purin-2,6-dion (Caffeine)

^{1}H NMR, 360 MHz, MeOH-d4, δ (ppm): 7.85 (1H, s), 3.97 (3H, s), 3.52 (3H, s), 3.34 (3H, s).

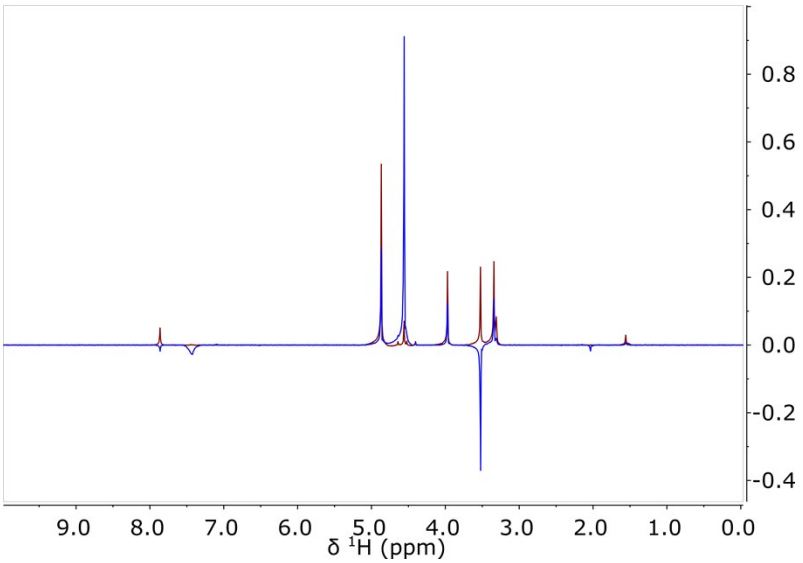

Figure S10: Comparison between a single scan ^{1}H spectrum of thermally polarized caffeine and a hyperpolarized experiment (blue). Note that caffeine concentration is only 23 mM (saturated in MeOH-d4. We observe an uncharacteristically large enhancement for the bound species resonance and the 7-methyl protons.

5) Field dependence of polarisation build-up

We initially found that non-zero enhancement are yielded at a magnetic evolution field of 65 G (6.5 mT), the characteristic field for the IMes catalyst (see Figure 9, enhancement 50, substrate 2-methylpyridine). We found that significant improvement could be obtained by increasing the field to roughly 140 G. In some cases, enhancements at 65 G are negligible (see Figure 10). We found that all compounds yield maximum signal at 140 G, which is roughly twice the characteristic evolution field required for [IrCl(COD)(IMes)] and consistent with observations by Pravdivtsev for ^{31}P containing catalysts.[30]

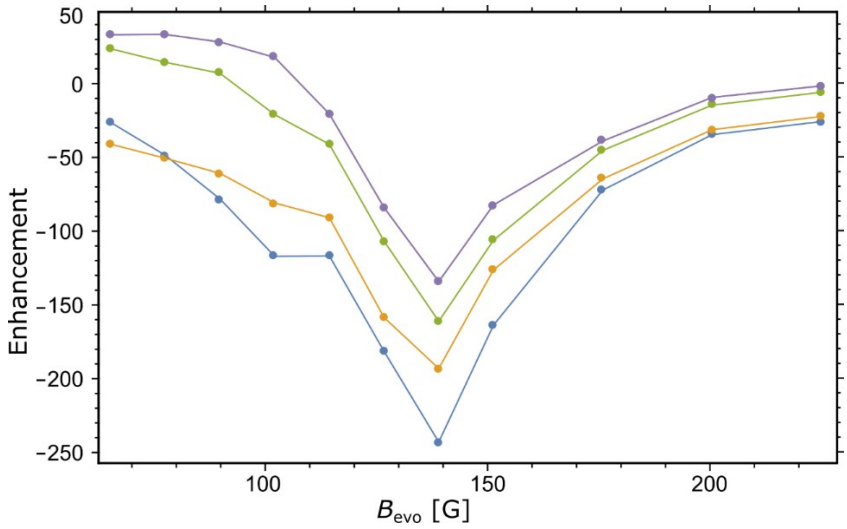

Figure S11: 2-Methylpyridine enhancements for the aromatic positions (blue H(6), yellow H(4), green H(5), purple H(3)). Aliphatic protons show no distinct field dependence (not shown), enhancement is about 10.

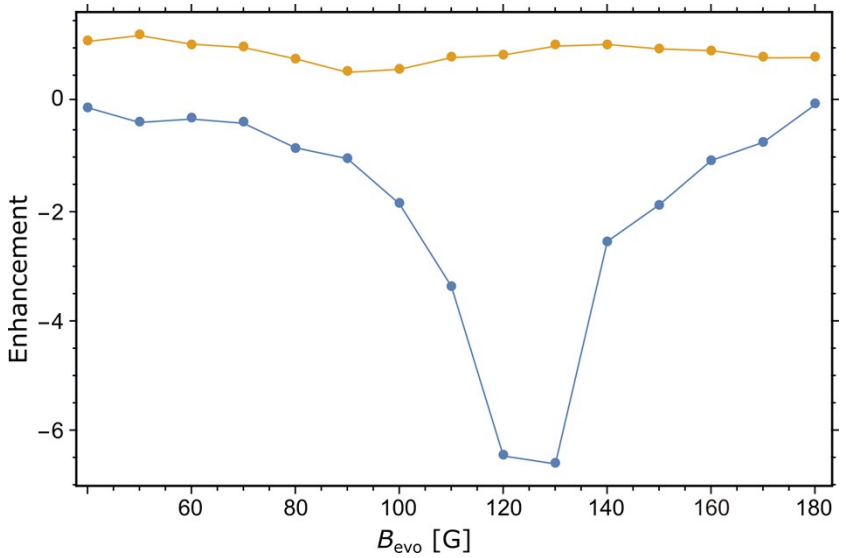

Figure S12: Enhancements for 2-methyl (yellow) and aromatic H(6) protons in pyridoxine (provitamin B6).

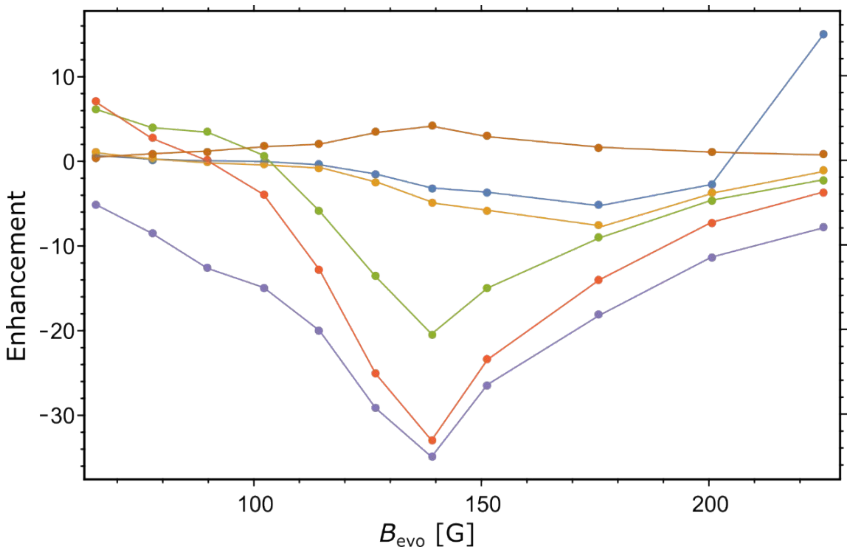

Figure S13: 2-Ethylpyridine enhancements for the 6 different resonances (purple H(6), red H(4), green H(5), yellow H(3), blue CH_2, orange CH_3). The largest enhancements are recorded for H(6), and H(4), followed by the meta*-hydrogen positions (5) and (3).*

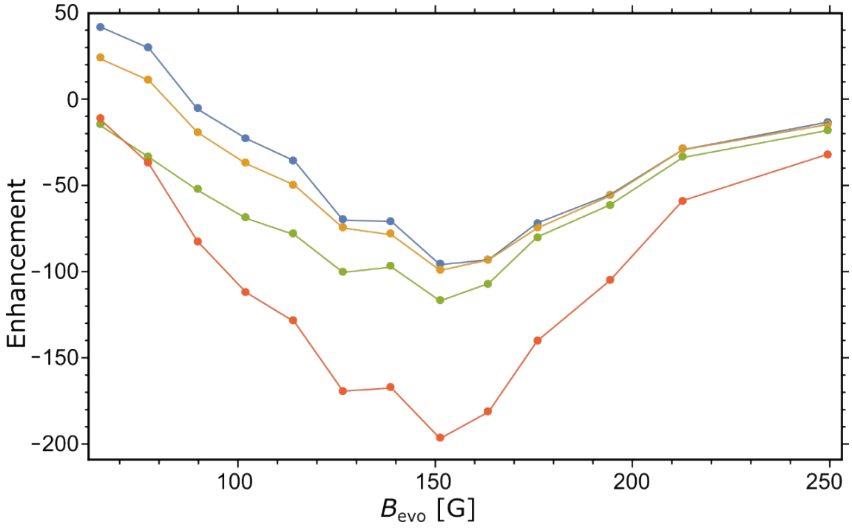

Figure S14: 2-Fluoropyridine enhancements for the 4 distinct resonances (red H(6), green H(4), yellow H(5), blue H(3)).

6. Application to other nuclei

The catalyst can also be utilized to hyperpolarize ^{15}N in the compounds investigated in the main article. We found that the majority of pyridine derivates, as well as our standard test substrate $CH_3C^{15}N$ are readily hyperpolarized. We found that elevated temperature is beneficial and allows to obtain larger levels of ^{15}N polarisation, optimum temperature is reached at 65 °C for Nitriles. Pyridine derivatives seem to require lower temperatures, however in lieu of ^{15}N labelled compounds a careful study could not be performed due to SNR restrictions.

Last, we attempted hyperpolarisation of ^{19}F in 2-fluoropyridine. In our study we swept the magnetic field over a large range, but enhancements generally remained low. A maximum enhancement of 30 was obtained at 5.4 mT matching field (see Fig. S15).

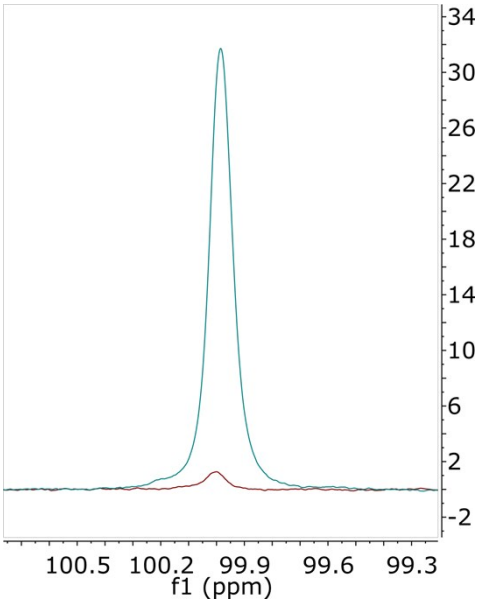

Figure S15: Comparison between a single scan ^{19}F spectrum of thermally polarized 2-Fluoropyridine (red) and hyperpolarized equivalent (light green) at room temperature. The enhancement is 30. The best signal is obtained at a matching field of 5.4 mT. Hyperpolarisation was conducted at room temperature.

7. H-D exchange in 2-fluoropyridine

For the 2-fluoropyridine substrate, H-D exchange was observed as noted in footnote **b** in Table 1 in the main paper. Figure S16 shows NMR data to demonstrate that the ortho-^{1}H disappears (red) after 30 minutes of activation (black is prior to activation).

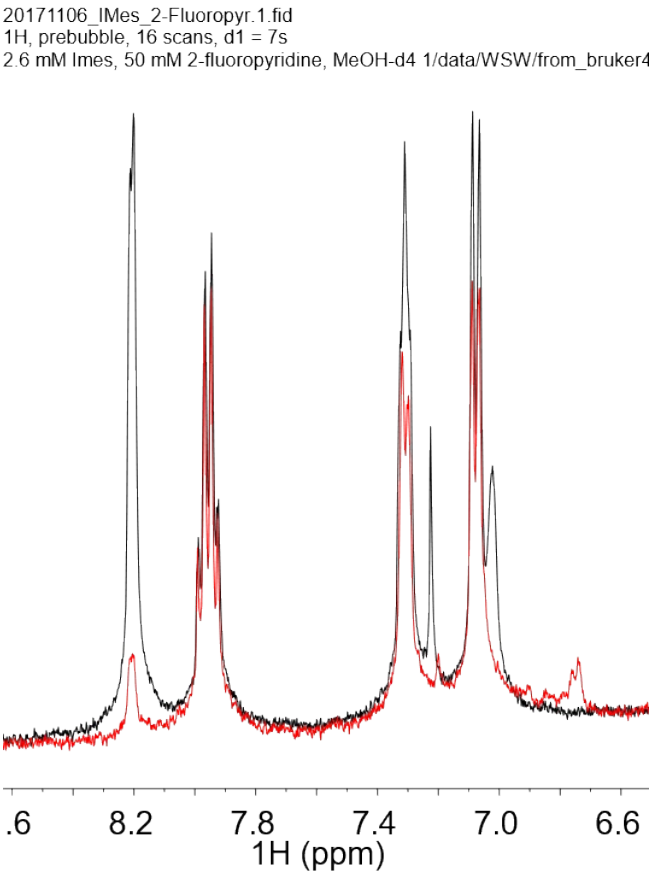

Figure S16: NMR signal demonstrating the decrease of ortho-^{1}H in 2-fluoropyridine due to H-D exchange. Black curve: Prior to activation. Red curve: After 30 min of activation. The peak at 8.2 ppm is associated with ortho-^{1}H, see, e.g., Spectral Database for Organic Compounds (SDBS), https://sdbs.db.aist.go.jp/sdbs/cgi-bin/direct_frame_top.cgi, compound number 13723 (retrieved on January 16, 2020).

References

1. K. Tani, D. C. Behenna, R. M. McFadden and B. M. Stoltz, *Organic Letters*, 2007, **9**, 2529-2531.
2. M. R. Krout, J. T. Mohr and B. M. Stoltz, *Organic Synth*, 2009, **86**, 181-181.
3. A. Y. Hong, N. B. Bennett, M. R. Krout, T. Jensen, A. M. Harned and B. M. Stoltz, *Tetrahedron*, 2011, **67**, 10234-10248.
4. B. Wüstenberg and A. Pfaltz, *Adv. Synth. Catal.*, 2008, **350**, 174-178.
5. V. Blum, R. Gehrke, F. Hanke, P. Havu, V. Havu, X. Ren, K. Reuter and M. Scheffler, *Comput. Phys. Commun.*, 2009, **180**, 2175-2196.
6. V. Havu, V. Blum, P. Havu and M. Scheffler, *Journal of Computational Physics*, 2009, **228**, 8367-8379.
7. X. Ren, P. Rinke, V. Blum, J. Wieferink, A. Tkatchenko, A. Sanfilippo, K. Reuter and M. Scheffler, *New Journal of Physics*, 2012, **14**.
8. K. Lejaeghere, G. Bihlmayer, T. Björkman, P. Blaha, S. Blügel, V. Blum, D. Caliste, I. E. Castelli, S. J. Clark, A. Dal Corso, S. de Gironcoli, T. Deutsch, J. K. Dewhurst, I. Di Marco, C. Draxl, M. Dułak, O. Eriksson, J. A. Flores-Livas, K. F. Garrity, L. Genovese, P. Giannozzi, M. Giantomassi, S.

Goedecker, X. Gonze, O. Grånäs, E. K. U. Gross, A. Gulans, F. Gygi, D. R. Hamann, P. J. Hasnip, N. A. W. Holzwarth, D. Iuşan, D. B. Jochym, F. Jollet, D. Jones, G. Kresse, K. Koepernik, E. Küçükbenli, Y. O. Kvashnin, I. L. M. Locht, S. Lubeck, M. Marsman, N. Marzari, U. Nitzsche, L. Nordström, T. Ozaki, L. Paulatto, C. J. Pickard, W. Poelmans, M. I. J. Probert, K. Refson, M. Richter, G.-M. Rignanese, S. Saha, M. Scheffler, M. Schlipf, K. Schwarz, S. Sharma, F. Tavazza, P. Thunström, A. Tkatchenko, M. Torrent, D. Vanderbilt, M. J. van Setten, V. Van Speybroeck, J. M. Wills, J. R. Yates, G.-X. Zhang and S. Cottenier, *Science*, 2016, **351**.

9. S. R. Jensen, S. Saha, J. A. Flores-Livas, W. Huhn, V. Blum, S. Goedecker and L. Frediani, *The Journal of Physical Chemistry Letters*, 2017, **8**, 1449-1457.
10. A. Tkatchenko and M. Scheffler, *Phys. Rev. Lett.*, 2009, **102**.
11. J. P. Perdew, K. Burke and M. Ernzerhof, *Phys. Rev. Lett.*, 1996, **77**, 3865-3868.
12. Y. Zhao and D. G. Truhlar, *Theor. Chem. Acc.*, 2007, **120**, 215-241.
13. M. Rossi, V. Blum, P. Kupser, G. Von Helden, F. Bierau, K. Pagel, G. Meijer and M. Scheffler, *Journal of Physical Chemistry Letters*, 2010, **1**, 3465-3470.
14. S. Chutia, M. Rossi and V. Blum, *Journal of Physical Chemistry B*, 2012, **116**, 14788-14804.
15. M. Rossi, S. Chutia, M. Scheffler and V. Blum, *The Journal of Physical Chemistry A*, 2014, **118**, 7349-7359.
16. F. Schubert, K. Pagel, M. Rossi, S. Warnke, M. Salwiczek, B. Koksch, G. von Helden, V. Blum, C. Baldauf and M. Scheffler, *Physical chemistry chemical physics : PCCP*, 2015, **17**, 5376-5385.
17. M. Ropo, M. Schneider, C. Baldauf and V. Blum, *Sci Data*, 2016, **3**, 160009.
18. N. Marom, A. Tkatchenko, M. Rossi, V. V. Gobre, O. Hod, M. Scheffler and L. Kronik, *Journal of Chemical Theory and Computation*, 2011, **7**, 3944-3951.
19. M. Sinstein, C. Scheurer, S. Matera, V. Blum, K. Reuter and H. Oberhofer, *J. Chem. Theory Comput.*, 2017, **13**, 5582-5603.
20. K. D. Atkinson, M. J. Cowley, P. I. P. Elliott, S. B. Duckett, G. G. R. Green, J. López-Serrano and A. C. Whitwood, *J. Am. Chem. Soc.*, 2009, **131**, 13362-13368.
21. C. Liu, W. Huhn, K.-Z. Du, A. Vazquez-Mayagoitia, D. Dirkes, W. You, Y. Kanai, D. B. Mitzi and V. Blum, *Physical Review Letters*, 2018, **121**, 146401.
22. M. K. Jana, C. Liu, S. Lidin, D. J. Dirkes, W. You, V. Blum and D. B. Mitzi, *Chemistry of Materials*, 2019, **31**, 8523-8532.
23. A. C. Whitwood, personal communication.
24. F. Maseras, A. Lledós, E. Clot and O. Eisenstein, *Chemical Reviews*, 2000, **100**, 601-636.
25. N. V. Belkova, L. M. Epstein, O. A. Filippov and E. S. Shubina, *Chemical Reviews*, 2016, **116**, 8545-8587.
26. G. G. Hlatky and R. H. Crabtree, *Coordination Chemistry Reviews*, 1985, **65**, 1-48.
27. T. Theis, G. X. Ortiz , A. W. J. Logan, K. E. Claytor, Y. Feng, W. P. Huhn, V. Blum, S. J. Malcolmson, E. Y. Chekmenev, Q. Wang and W. S. Warren, *Science Advances*, 2016, **2**.
28. J. F. P. Colell, A. W. J. Logan, Z. Zhou, R. V. Shchepin, D. A. Barskiy, G. X. Ortiz, Q. Wang, S. J. Malcolmson, E. Y. Chekmenev, W. S. Warren and T. Theis, *J. Phys. Chem. C*, 2017, 6626–6634.
29. J. F. P. Colell, M. Emondts, A. W. J. Logan, K. Shen, J. Bae, R. V. Shchepin, G. X. Ortiz, P. Spannring, Q. Wang, S. J. Malcolmson, E. Y. Chekmenev, M. C. Feiters, F. P. J. T. Rutjes, B. Blümich, T. Theis and W. S. Warren, *J. Am. Chem. Soc.*, 2017, **139**, 7761-7767.
30. A. N. Pravdivtsev, A. V. Yurkovskaya, H.-M. Vieth, K. L. Ivanov and R. Kaptein, *Chem. Phys. Chem*, 2013, **14**, 3327-3331.